Chapter 13
Dynamic Analysis of a Modular Test Stand for Multi-Axis Vibration Testing

H. R. Kramer, J. F. Schultze, S. M. Danforth, and B. P. Mann

Abstract This study investigates a modular test stand, designed to support multi-axis vibration testing, that uses three orthogonal electrodynamic shakers. To capture the effects of shaker-stand interaction, the dynamics of the test stand were analyzed in three unique configurations. The modal characteristics of the test stand in each configuration were extracted via roving hammer impact tests. The approximate transmissibility between various points on the test stands indicated that all three configurations were compliant in the frequency range of interest. Additionally, multiple-input, multiple-output (MIMO) random vibration tests (RVT) were performed on a basic geometry with well-defined dynamics. These MIMO tests analyzed the degree of coupling between the test article and the respective test stand configurations. Examination of the control power spectral densities and inverse frequency response functions revealed that the test stand configuration had no noticeable effect on the performance of the MIMO tests. Furthermore, the resonances of the test article were the main contributor to poor controller performance.

Keywords Test Stand · MAVT · RVT · Modal Analysis · MIMO

Introduction

When attempting to replicate a random vibration environment via ground testing, two common excitation methods are single-axis and multi-axis testing. Multi-axis vibration testing (MAVT) has gained interest in the dynamic environment testing community due to its more realistic environmental replication when compared to traditional single-axis testing. However, MAVT comes with additional design challenges and more complex test setups. When performing single-axis testing, the test article is excited and controlled one axis at a time, often using one large shaker or slip table. Conversely, multi-axis testing aims to excite and control a test article in multiple axis simultaneously, requiring multiple shakers and a test stand. Some work has been done to optimize shaker attachment and response measurement locations for multiple-input, multiple-output (MIMO) vibration tests in [1, 2]. However, every unique test article can result in different optimal shaker attachment points, thereby necessitating a test stand that is modular, easy to assemble, and cost-effective.

Recent advancements in MAVT, such as impedance matched multi-axis testing (IMMAT) [3], have shown that boundary conditions are an important consideration to achieve realistic environmental excitation. Boundary conditions are commonly influenced by test article fixturing and shaker attachment. When a test article is attached to a shaker via a stinger, some shaker-structure interaction will occur. This interaction couples the dynamics of the shaker and stinger to the dynamics of the structure. Shaker-structure coupling can introduce unwanted dynamics to the system, and in turn leads to unrealistic responses. Research has been done to understand this phenomenon in [4, 5, 6, 7, 8] and practical considerations are discussed to mitigate its effects in [9]. However, less published work has been directed toward understanding the dynamics between the shaker and test stand.

Within distributed shaker test setups, methods for positioning shakers include suspending the shakers from or mounting the shakers to a test stand. Suspending the shaker using a bungee reduces the coupling between the shaker and test stand, but

H. R. Kramer · B P Mann
Department of Mechanical Engineering and Materials Science, Pratt School of Engineering, Duke University, NC 27708
e-mail: hunter.kramer@duke.edu; brian.mann@duke.edu

J. F. Schultze · S. M. Danforth
Los Alamos National Laboratory, NM 87545
e-mail: schultze@lanl.gov; sdanforth@lanl.gov

Alexandra Karlicek et al. (eds.), *Dynamic Environments Testing, Vol. 7*, Conference Proceedings
of the Society for Experimental Mechanics Series, https://doi.org/10.13052/97887-438-0152-8_13

also reduces the force that can be transmitted to the test article. When attempting to replicate more rigorous test specifications, such as flight-relevant environments, the shaker may push itself away from the test article instead of producing the desired environment. Alternatively, the shaker can be rigidly mounted to a test stand. With a rigid structure to push from, the shaker is capable of transmitting a larger force than if it were suspended. However, when the shaker is rigidly attached to the test stand, the shaker and stand become more dynamically coupled. This coupling can introduce unwanted test stand resonances into the MAVT, thus decreasing control quality.

The goal of this study was to measure the effect of test stand dynamics on a sample MIMO vibration test. We first introduce a modular test stand designed to support distributed shaker MAVT with three orthogonal electrodynamic shakers directly mounted to the stand. To understand and possibly mitigate the effects of shaker-stand interaction, we investigated the dynamics of the test stand via modal analysis for the three test stand configurations. Once the dynamics of the test stand and test article were understood, we conducted a MIMO random vibration test for each configuration. The MIMO tests provided a means of assessing the degree of coupling between the test stand and test article.

The remainder of this paper is organized as follows: The three test stand configurations are introduced, followed by an analysis of their dynamics via modal testing and transmissibility considerations. Our MIMO test setup is then described and the results of these tests are discussed. The results are summarized in the discussion/conclusion section, followed by the references and the appendix. The appendix contains the modal frequencies of the three test stand configurations and test article.

Test Stand Configurations

This study examines the dynamics of three unique test configurations. Our first configuration was the original design, referred to as the "Undamped" configuration, and is shown in Figure 1a. We developed our test stand using the Creo Parametric CAD suite. In the CAD design phase, the test stand was iterated upon based on design review feedback from our team. Our design requirements led to a simple, modular, and cost effective test stand. Our finalized design utilized t-slot framing with accompanying hardware that is readily available from hardware suppliers.

Our original design consisted of three compartments, each approximately 1'x1'x3'. The center compartment housed the test article and was spacious enough to mount a 50 lb shaker oriented in the Z-axis (not depicted). The two side compartments, adjacent to the center compartment, provided space for smaller, 7 lb Modal Shop shakers. Our smaller shakers were mounted via their trunion to a rigid aluminum plate. We then mounted the aluminum base plate to the test stand using t-slot hardware. As depicted in Figure 1, the shaker platforms were installed halfway up our vertical beams (1.5'). Our hardware selection facilitated quick reconfiguration, allowing for the small shakers to be moved in three axes. This flexibility was intended to eliminate the need to disassemble or redesign the stand when testing different structures.

To improve upon our initial design, we investigated ways to add stiffness and damping to the test stand. We hypothesized that making the test stand stiffer and more damped would help mitigate the effects of test stand dynamics on the test article. Two subsequent test stand configurations were developed to test this hypothesis. Our first subsequent configuration, referred to as the "Damped" configuration, utilized anti-slip rubber inserts to add damping. We added damping material to one side of every beam in the test stand, however, some locations required extra damping. We evaluated where to add extra damping

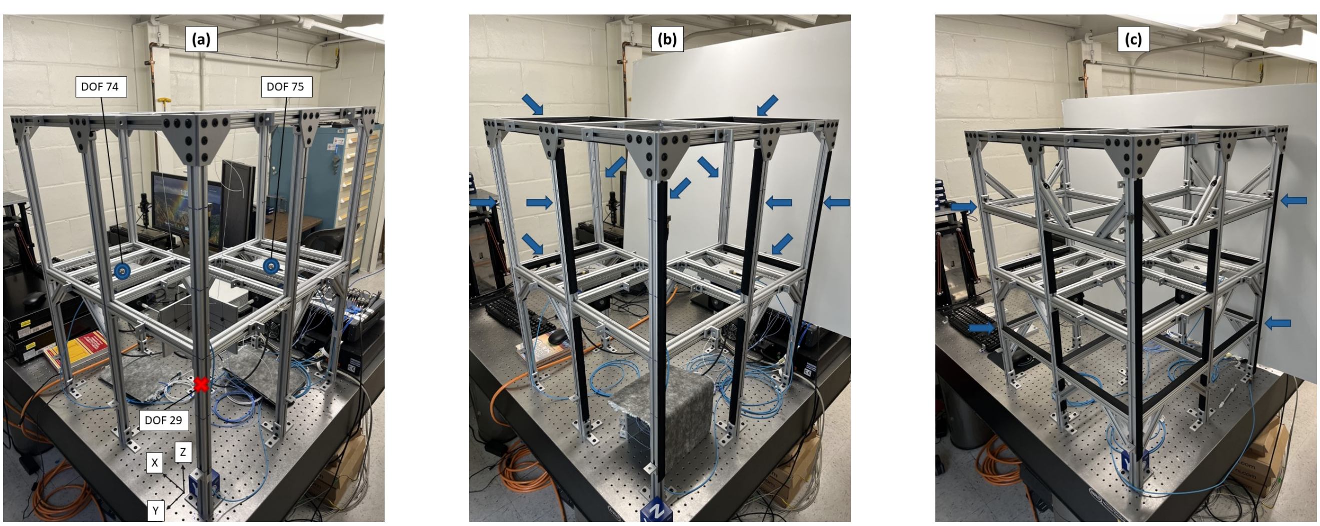

Fig. 1 The three test stand configurations: (a) undamped, (b) damped, (c) stiffened

by impacting the structure with a metal object and listening for an audible ring. The top and middle horizontal platforms were identified via this method to have excessive ringing, and therefore received damping on two sides instead of one. The eight vertical beams and two platforms of our structure where damping material was added are denoted with blue arrows in Figure 1b. Our second subsequent configuration, referred to as the "Stiffened" configuration, aimed to increase the stiffness of the test stand and is shown in Figure 1c. We added horizontal stiffeners and 45° gussets to reduce the distance between supports from 1.5' to 0.75'. As a result, two additional platforms were created and are denoted by blue arrows in Figure 1c. We evaluated the new platforms for excessive ringing and added damping material via the previously described method.

Modal Analysis

To determine the dynamics of the three configurations (undamped, damped, and stiffened) we performed roving hammer impact tests. During each impact test, the small 7 lb shakers were attached to the test stand, but the test article was not. We utilized the Siemens Testlab 2021.2.1 Impact Testing module to estimate frequency response functions (FRFs) for each configuration. These FRFs were then exported to ATA's IMAT 8.1.0 suite to compute the mode shapes via the OPoly application. Each impact test consisted of 78 points excited in three axes, X, Y, and Z. Altogether, we calculated the mode shapes using responses from 234 degrees of freedom (DOFs) for each test stand configuration. To excite the structure in the axial direction of each beam, we installed a 1"x1" L-bracket on the test stand. We then impacted the L-bracket in the axial direction of the beam, allowing for a full modal model to be developed. Between DOFs, we loosened the L-bracket and moved it to the next DOF along the same beam. We recognize that moving the L-bracket between impacts could affect the dynamics of the structure. However, we assumed that the weight of the 1"x1" L-bracket was negligible in comparison to the weight of the test stand.

Our planned MIMO test had a frequency range of 20-2000 Hz. As such, we attempted to obtain the test stand modes up to 2000 Hz for each configuration. Unfortunately, the test stand had many more modes than we initially anticipated. Due to the modal density, we were only able to resolve mode shapes up to 300Hz. In this reduced range, 20-30 modes were extracted, depending on the test stand configuration. To validate our extracted mode shapes, we employed the modal assurance criterion (MAC).

From theory, the modes of a given structure will have unique shapes and corresponding frequencies, except for symmetric geometries which may exhibit repeated roots (such as geometries with square or circular cross sections). The MAC provides an effective means of comparing the similarity of one mode shape to another. The MAC between the m^{th} mode of structure A, $\{\Psi_A\}_m$, and the n^{th} mode of structure B, $\{\Psi_B\}_n$, is calculated as

$$MAC(m,n) = \frac{\left| \{\Psi_A\}_m^T \{\Psi_B\}_n^* \right|^2}{\left(\{\Psi_A\}_m^T \{\Psi_A\}_m^*\right)\left(\{\Psi_B\}_n^T \{\Psi_B\}_n^*\right)} \tag{1}$$

where the superscript T denotes the transpose and the superscript $*$ denotes the complex conjugate. An "ideal" MAC for a single structure with no repeated roots would show all off-diagonal terms to be 0 (all mode shapes are dissimilar to each other) and all diagonal terms equal to 1 (each mode shape is perfectly similar to itself). In this work the MAC scores are shown as percentages, ranging from 0-100 instead of 0-1. It should be noted that for MACs that compare one structure to another, the "ideal" criteria are not the same. A brief review of the MAC and its applications are provided in [10].

A representative sample of MAC scores for each tests stand configuration are shown in Figure 2. All MAC scores shown in Figure 2 correspond to modes under 130 Hz. For the interested reader, all extracted modal frequencies for the three test stand configurations are displayed in Table 4 of the appendix.

A keen eye will discern that our extracted mode shapes were not perfectly orthogonal. Take, for example, the MAC scores for modes 9 and 10 of the stiffened configuration shown in Figure 2c. The MAC score between these two modes indicates that they were 75% similar. Upon inspection of these mode shapes, it was observed that these two modes were similar, but distinct. High MAC scores in the off-diagonal can result from a number of sources. Incorrect mode selection, spatial aliasing, poor signal to noise, or frequency spacing that is too coarse are common sources. In the case of mode 9 and 10 of the stiffened configuration, we noticed that the impact measurements were noisy and that our frequency spacing may have been too coarse. These two factors led to difficulty resolving modes 9 and 10 using using the OPoly application. Despite these challenges, we deemed the MAC plots seen in Figure 2a-c to be acceptable for this study.

The MAC scores in Figure 2 allowed us to analyze how the dynamics of the test stand changed in each configuration. It was observed that the damped configuration had six additional modes in the same frequency range as the undamped configuration. Using the MAC to compare the mode shapes between the undamped and damped configurations, as seen in Figure 2d, these findings can be investigated.

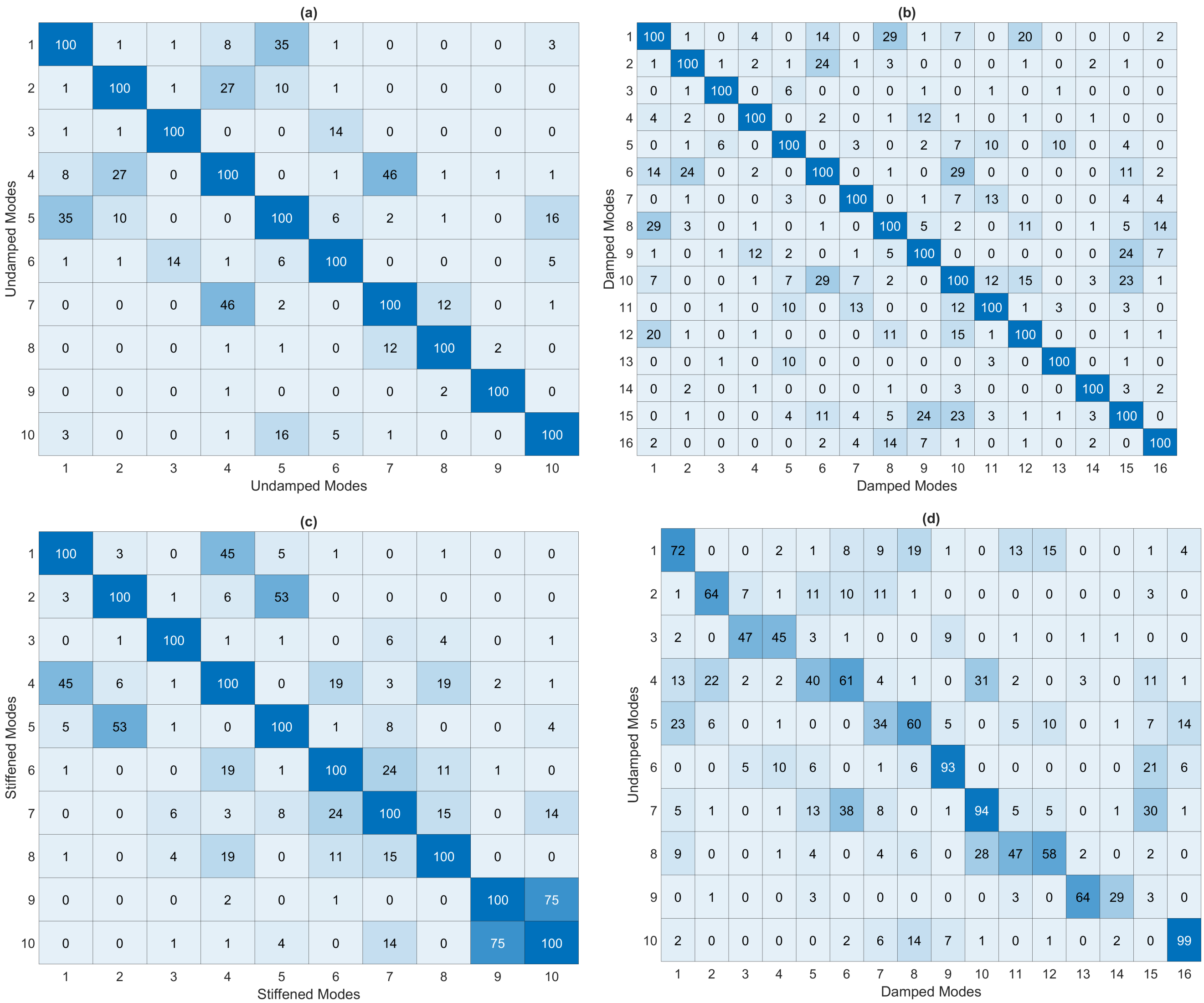

Fig. 2 The modal assurance criterion scores (experimental to experimental) for the three test stand configurations: (a) undamped, (b) damped, (c) stiffened, (d) undamped vs damped

When damping is applied to a system, a single mode can be split into two, lower amplitude modes. Each of the two resultant modes exhibit part of the behavior of the original mode shape. In Figure 2d mode splitting was observed between the undamped and damped configurations. Specifically, modes 3, 4, 5, 8, and 9 of the undamped configuration appear to have split, corresponding to the main diagonal of Figure 2d being stretched along the X-axis. Visual inspection of the extracted mode shapes were consistent with this finding, providing an explanation for five of the six additional modes. The last additional mode, mode 15 of the damped configuration, had very low similarity with any nearby modes. Aside from mode splitting, spontaneous addition of a mode is another potential result of changing the dynamics of a structure (such as adding damping). From this analysis, it can be concluded that the dynamics of the test stand shifted by a measurable amount due to the changes we made.

Transmissibility Analysis

The modal data from our impact tests were useful for identifying dynamic changes between test stand configurations. However, the relative motion between points on the structure was also of interest. One metric that can be useful for understanding relative motion between DOFs is transmissibility. Transmissibility (TR) can be derived using several methods, leading to slightly different interpretations. To avoid ambiguity, a brief review of how we calculated transmissibility is described.

The preferred method for calculating TR is to use spectra obtained from time data. In this method, the TR between response spectra from two DOFs (as opposed to one input DOF and one output DOF for FRFs) is computed using an FRF estimator, such as the H1 method. Doing so reduces the effect of noise on the input (uncorrelated noise will average out). However, we did not have access to the time data from our impact testing. Alternatively, we used a less optimal, FRF-based method. In this method, the TR is approximated using the FRFs for the two response DOFs, and only the resultant magnitude is considered. Suppose an FRF estimate exists between an input at DOF, F, and an output at DOF, X. Using the H1 method, the FRF estimate, H_{XF} is calculated by

$$H_{XF} \approx \frac{G_{XF}}{G_{FF}} \approx \frac{S_X}{S_F} \tag{2}$$

where G_{XF} is the cross power between X and F, G_{FF} is the auto-power of F, S_X is the linear spectra of X, and S_F is the linear spectra of F. Let's assume that an FRF estimate exists for another point, Y, using the same input F. Using the FRF for DOF X, H_{XF}, and the FRF for DOF Y, H_{YF}, the TR between DOF X and Y can be estimated by

$$T_{XY} \approx \frac{H_{XF}}{H_{YF}} \approx \frac{G_{XF}}{G_{FF}} / \frac{G_{YF}}{G_{FF}} \approx \frac{G_{XF}}{G_{YF}} \approx \frac{S_X}{S_Y}. \tag{3}$$

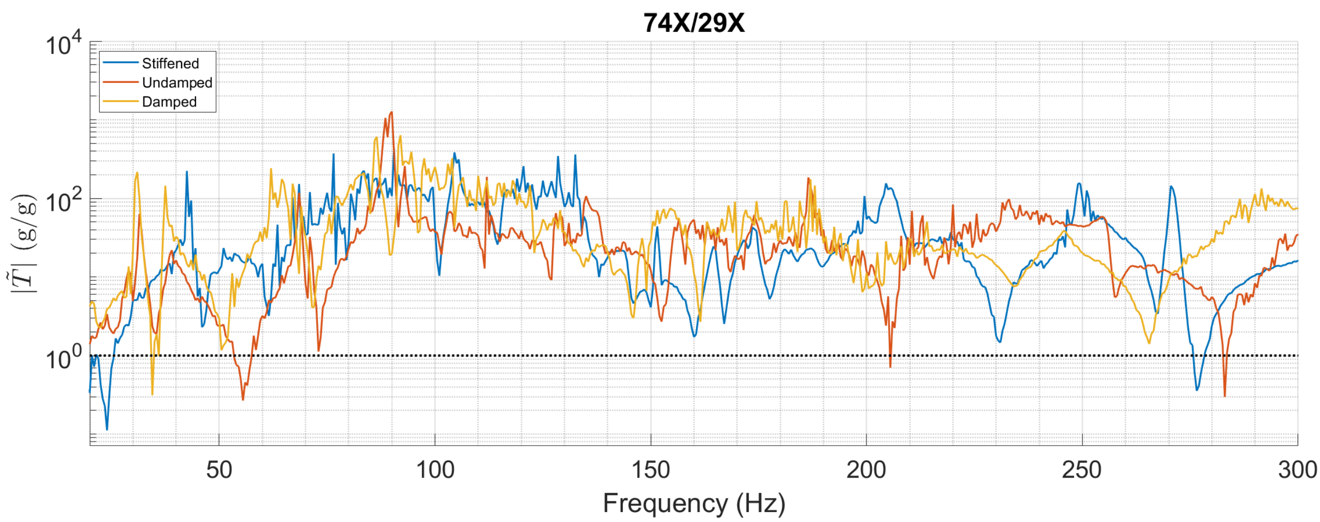

Fig. 3 The approximate transmissibility between the base of the test stand and the shaker attachment point for all three test stand configurations, with a horizontal dotted line added at 10^0 for clarity

Equation 3 shows that the contribution from the input F cancels out and thus leaves the TR between DOF X and Y. In theory, the noise from the G_{FF} cancels out of this estimate. However, in practice, there is always some residual error from the noise. Additionally, this method fails when the applied force approaches zero, indicating a force dropout in the data. With these limitations in mind, the approximate TRs between the test stand configurations were analyzed.

Ideally, shakers rigidly attached to a test stand would allow for the transfer of force without introducing unwanted dynamics. To estimate the deviation of our test stands from this idealization, we examined the magnitude of the approximate TR between the base of the test stand, and the shaker attachment point. For a perfectly rigid test stand, the magnitude of the TR between the base and the shaker equals 1, corresponding to zero relative motion between them. Figure 3 shows the approximate TR between a sample shaker mounting DOF, 74X, and a sample base point of the test stand, 29X. Both locations are denoted in Figure 1a. Note that DOF 29X was located behind the vertical beam in the foreground of Figure 1a and was indeed a foot of the test stand.

The TR depicted in Figure 3 indicates that our test stand was far from rigid. In fact, in the range of our modal analysis, relative motion was observed on the order of 10^3 between the base of the test stand and where the shaker was mounted. Relative motion of this magnitude indicates that our test stand was very compliant in this range. This finding indicates that for all three test stand configurations, the dynamics of the test stand affected the shakers, and may have affected the test article.

In addition to the approximate TR between the shaker locations and the base of the test stand, we also investigated the relative motion between the two shaker locations. Ideally, the magnitude of the TR between these two DOFs would be close to 1, indicating that the shakers will not move relative to each other. Relative motion between the shakers can induce a moment on the test article or reduce the force transmitted through the stingers.

Figure 4 shows the approximate TR between the two shaker locations. We chose DOF 74X and DOF 75Y for this analysis because they were the shaker drive DOFs and are denoted in Figure 1a. High TR between these two DOFs indicates that the shakers, in the direction of the applied force, were moving relative to each other. Figure 4 shows that the relative motion between shakers was much less severe than the motion between the shakers and the base. However, there was still relative motion on the order of 10^2 between them in the range of 100-150 Hz. Adding stiffness to the test stand positively affected the TR in both of our comparisons, pushing the TR curves down toward 1. Therefore, we predicted that the stiffened configuration would have better control performance in the MIMO test.

Our analysis of the mode shapes and approximate TRs of our test stand indicated that dynamic interaction between our test stand and shakers was likely. To ascertain the degree of interaction, we performed MIMO vibration tests in each test stand configuration. The following section introduces our test article and details how we performed our MIMO tests.

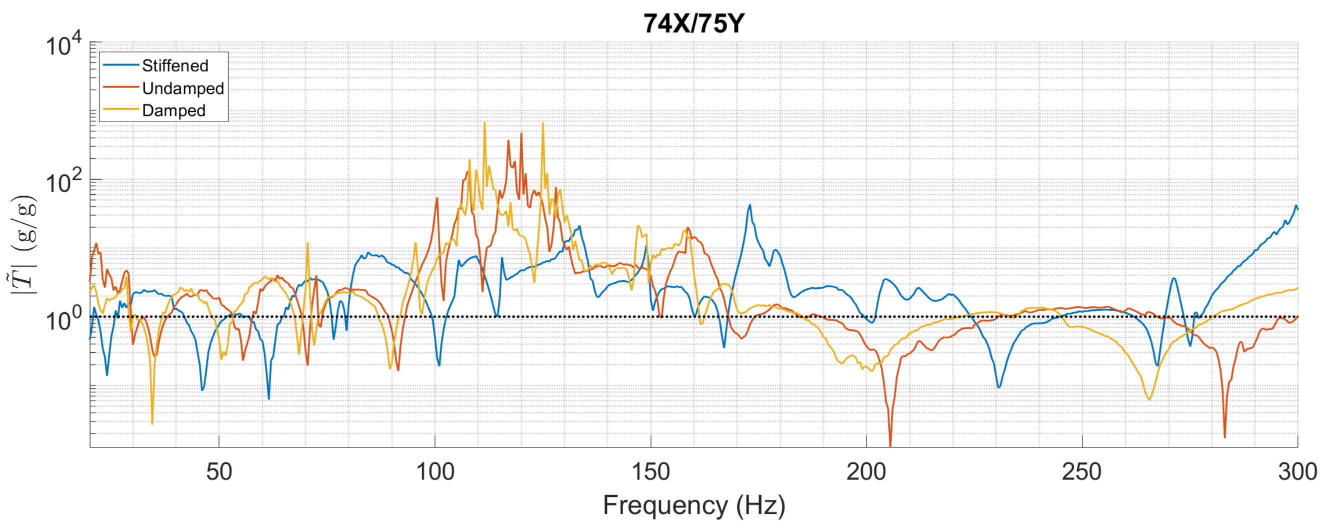

Fig. 4 The approximate transmissibility between the two shaker attachment points for all three test stand configurations, with a horizontal dotted line added at 10^0 for clarity

MIMO Test Setup

An appropriate test article is required to perform a MIMO test. We chose our test article based on two design requirements. The test article needed to have a simple geometry and well-defined dynamics. With a plethora of commercially available options, we chose an aluminum angle and iterated on the dimensions to ensure the test article had interesting dynamics in our frequency range of interest. From a finite element analysis (FEA), eight modes between 20-2000 Hz were expected. We confirmed these expectations through impact modal testing, where the test article was suspended by a fishing line to simulate a free-free boundary condition. The modal frequencies extracted from our impact test were within 5% of our FEA modes. We also visually compared the corresponding mode shapes and observed good agreement. The dimensions of the test article were 6”x6”x6”, with a thickness of 1/4”. We applied a grid of test points to the test article at a 2” spacing, except at the center line, where we applied a 1” spacing. The location of these grid points were informed by our FEA, and led to well-resolved mode shapes (as evidenced by our MAC in Figure 5c).

The test article, referred to as the Aluminum Angle (AL angle), was easily procured, with a shape that was conducive to attaching two orthogonal shakers (one on each wing). Figure 5 shows the AL angle in several orientations and the computed MAC from our modal analysis. The modal frequencies for the AL angle are listed in Table 4 of the appendix. The lowest mode occurred around 320 Hz. Since the range of our modal test on the test stands was limited to 300Hz, the dynamic effects from the test stand and the test article could be distinguished. We also note that the modal damping calculated for each AL angle mode was on the order of 0.01. Test articles with low damping such as our AL angle are challenging to control.

The goal of our study was to understand how the dynamics of our test stand affected MIMO testing. We developed a sample test specification with sufficient spectral energy to excite the modes of the test article. The control range for our

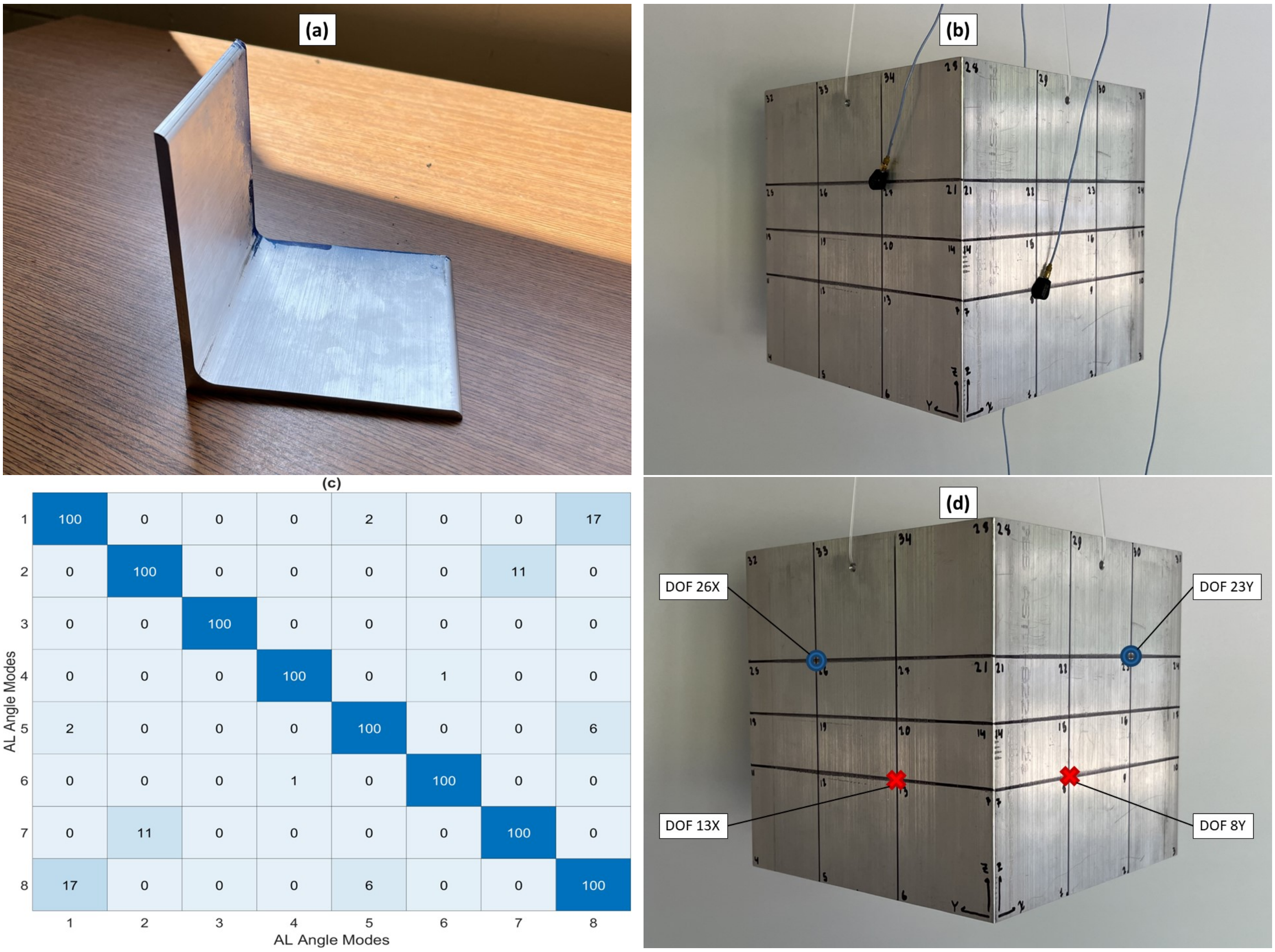

Fig. 5 The test article used in our MIMO tests: (a) AL Angle, (b) AL angle in the modal test configuration, (c) AL angle modal assurance criterion scores (experimental to experimental), (d) the AL angle in the MIMO test configuration

MIMO test was 20-2000 Hz. In the Testlab 2021.2.1 MIMO Random module, the lower end of the control range may not be a whole number (depending on the desired frequency resolution), leading us to develop a specification that started just below 20 Hz. Table 1 shows the breakpoints chosen for our test specification.

Table 1 The test specification breakpoints used for both control DOFs in our MIMO tests

Frequency (Hz)	**Magnitude** (g^2/Hz)
18	$1 \cdot 10^{-4}$
50	$2 \cdot 10^{-4}$
1000	$2 \cdot 10^{-4}$
2000	$1 \cdot 10^{-4}$

Our MIMO test utilized two shakers oriented in the X and Y directions as shown in Figure 6. We attached each shaker to the test article using a nylon stinger with an aluminum sheath. The stinger was then screwed into a force transducer, which we rigidly attached to the test article using super glue. Directly opposite the force transducer, control accelerometers were instrumented on the test article. Our choice of shaker attachment locations on the test article was informed by the experimental modal test. Locations lying on nodes of the modes were excluded to ensure adequate excitation of all the modes of our test article. Using engineering judgement, DOF 26X and 23Y were selected as the shaker attachment points and are denoted with blue circles in Figure 5d. Two additional response locations were instrumented at DOF 13X

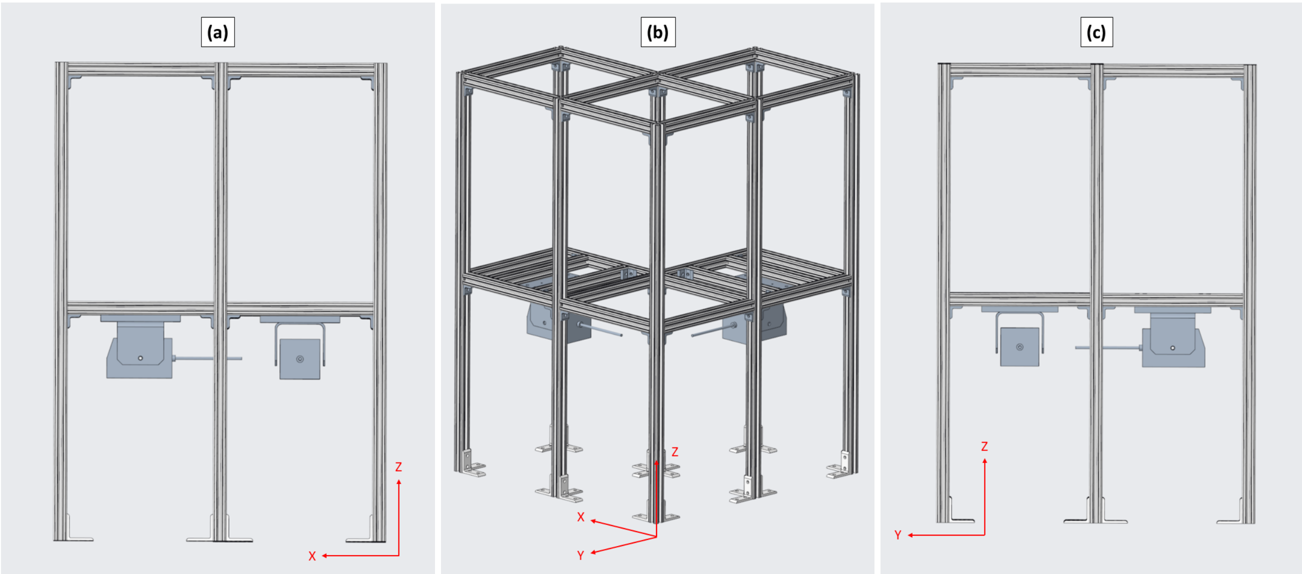

Fig. 6 The CAD model for the undamped test stand configuration with the 45° gussets removed: (a) left view, (b) isometric view, (c) right view

and 8Y to analyze the behavior of the test article at uncontrolled locations. The two response locations are denoted with red X's in Figure 5d. The triaxial accelerometers used during our modal test on the test stand (DOFs 74 and 75) were retained for our MIMO tests. Using these accelerometers, we were able to measure the response of the test stand, if any, at the shaker attachment points. Figure 1a shows the test article set up for the MIMO test in the undamped test stand configuration.

In the Testlab 2021.2.1 MIMO Random module, the user has the option to choose between control modes. In the PSD control mode, the controller ignores the cross power spectral density (CPSD) terms and only controls to the specified PSDs. An alternative control mode is "Matrix" control. In this mode, the controller attempts to control the system to specified CPSDs and PSDs. Our test specification did not include CPSDs, so PSD control was selected.

The sequence of tests followed a consistent pattern: The test stand configuration was assembled, a modal test was performed on the test stand, the test article was attached to the test stand, and then MIMO tested. Between assembly of the test stands, the test article was dismounted and set aside, allowing for easier assembly of the next test stand configuration. In an effort to keep the boundary conditions of the test article consistent with the modal test, we suspended the test article with fishing line for the MIMO tests. Wax was used to mount sensors to the test article, and accelerometers disturbed by removing and re-mounting the the test article where reseated as needed. The wax used in this study was sufficient up to 2000 Hz, and was chosen over a stronger adhesive to extend the life of the accelerometers.

MIMO Test Results

For the undamped and damped test configurations, the MIMO tests were performed successfully. However, when we performed the MIMO test in the stiffened configuration, an audible rattling could be heard around 1200 Hz. In addition to the rattling, we observed excessive twisting and displacement of the test article. We made several attempts to eliminate the twisting and displacement but were ultimately unsuccessful. Because there were no safety issues with this rattling, we adjusted the percentage of frequency lines that could violate the alarm (± 3 dB) and abort (± 6 dB) limits to allow the stiffened MIMO test to run. As a result, the full test was completed but exhibited poor low-frequency control. In searching for methods to reduce rattling, we truncated the specification to 20-1200 Hz and re-ran the stiffened MIMO test. Truncating the higher frequencies resulted in adequate low-frequency control. The results from the truncated MIMO test will be referred to as"Stiffened/Truncated." However, the results from the stiffened 20-2000 Hz MIMO test were retained for completeness.

Control Comparison

It is common practice when comparing random vibration tests to plot the control PSDs for each test against one another. Figure 7 plots the control PSD curves for all four MIMO test cases: undamped, damped, stiffened, and stiffened/truncated. Along with the PSD curves, the test specification, alarm (±3dB), and abort (±6dB) lines are plotted. The first row of Figure 7 compares each of the full bandwidth tests against each other. The second row compares only the stiffened test to the stiffened/truncated test. Each column of Figure 7 plots the control curves for a specific control DOF.

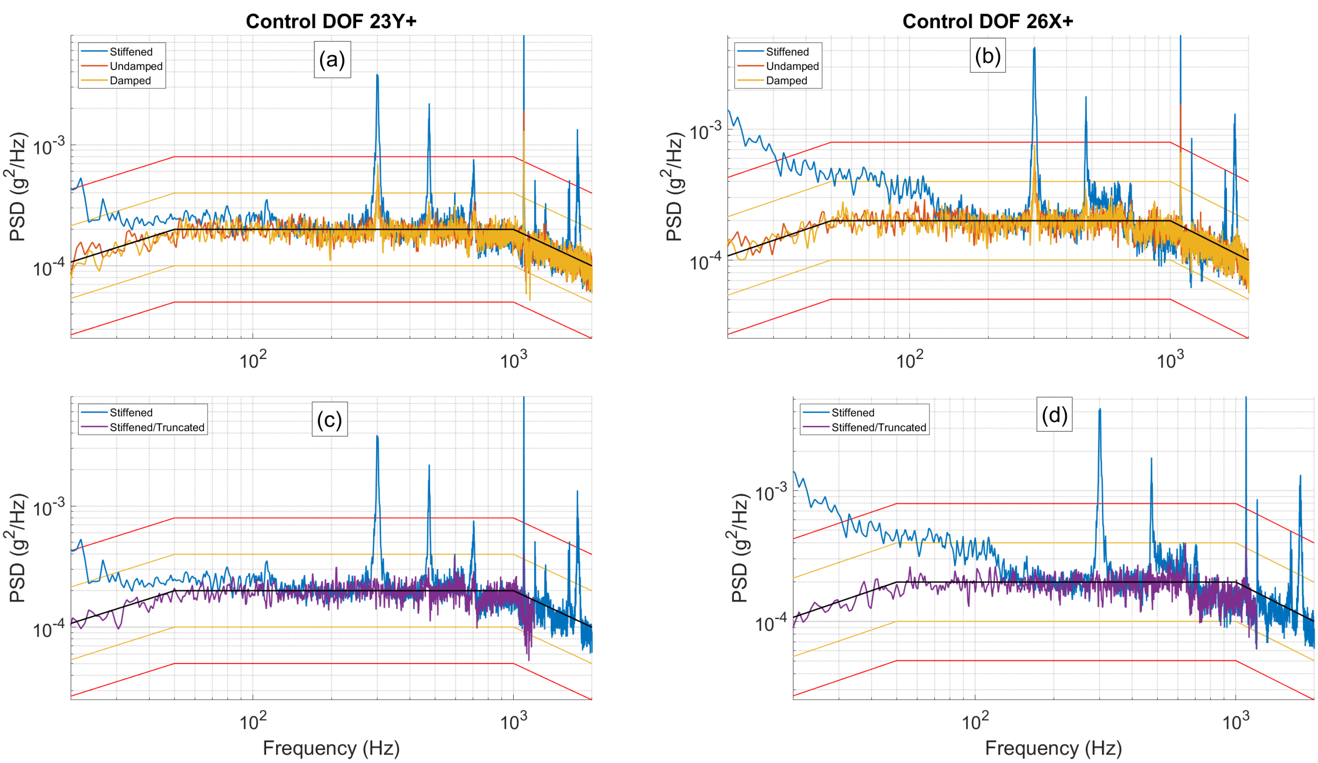

Fig. 7 The control PSD curves from the various MIMO tests. (a): undamped vs damped vs stiffened control at DOF 23Y+, (b): undamped vs damped vs stiffened control at DOF 26X+, (c): stiffened vs stiffened/truncated control at DOF 23Y+, (d): stiffened vs stiffened/truncated control at DOF 26X+

In Figure 7, the control PSDs for the undamped and damped configurations are nearly indistinguishable. One small difference is that the damped configuration displayed a small decrease in the peak seen around 1100 Hz. The stiffened control curve shows the greatest deviation from the test specification, as was expected with the issues we encountered.

The MIMO controller did not appear to have any issues controlling the test article between 20-300 Hz (excluding the stiffened configuration). Despite the multitude of test stand modes in this range, the control PSDs were well within the alarm limits. While the test stand modes seemed to have little impact on the MIMO control, the control was poor near the modes of the test article. The peaks in the PSD curves violated the abort limits at the following frequencies: 300 Hz, 475 Hz, 1096 Hz, 1208 Hz, 1624 Hz, and 1771 Hz. These peaks did not line up exactly with these test article modes, but were reasonably close (with the exception of 1208 Hz, where the rattle was observed). It is not uncommon for shaker-structure interaction to introduce slight dynamic changes to the test article. Therefore, it is reasonable to assume that some of the free-free modes of the AL angle may have shifted. Interestingly, the test article modes did not seem to pose a challenge for the controller in the stiffened/truncated case. The test stand did not change between the stiffened and stiffened/truncated MIMO tests, so the difference in performance was due to changes in the test article or control setup. One caveat to the stiffened/truncated MIMO test was the limited frequency range. Limiting the number of frequencies the controller must manage at any given time creates an easier control problem to solve.

It is difficult to differentiate the performance of similar control curves without some sort of metric. While limited, some standards do exist for comparing the performance of MIMO tests. One such standard found in MIL-STD-810H [11] is the acceleration root mean squared (gRMS) error. The gRMS error is used to determine the percent difference between the gRMS of the test specification, and the achieved control. The gRMS error was calculated using

$$gRMS_{Error} = \frac{|gRMS_{Spec} - gRMS_{Control}|}{gRMS_{Spec}} \cdot 100 \tag{4}$$

where $gRMS_{Spec}$ is the gRMS of the test specification, and $gRMS_{Control}$ is the gRMS of the achieved control. The lower the gRMS error score, the closer the control was to achieving the test specification. Table 2 displays the % gRMS error for each MIMO test at each control DOF.

The data in the far right column of Table 2 has been shaded based on performance of the respective test. Cells highlighted in green had better performance, while cells highlighted red had poorer performance. Unsurprisingly, the stiffened MIMO test overshoots the test specification by a wide margin. Analyzing the remaining MIMO test, it was observed that the damped MIMO test had the best performance. However, the % gRMS error between the the undamped, damped, and stiffened/truncated MIMO test only vary by about 3%. The threshold for gRMS error from MIL-STD-810 is ±10%. The undamped, damped, and stiffened/truncated MIMO tests were well below this threshold. This finding was surprising considering the dynamic differences between the test stand configurations.

The next metric applied to the data was the abort/alarm violation error. While not found in a published standard, this metric is commonly used in the Department of Energy (DOE) complex. When performing a MIMO test in Testlab 2021.2.1, abort and alarm lines are plotted with the test specification and measured control. The abort and alarm lines correspond to ±6dB and ±3dB from the test specification respectively. Applying a threshold for abort/alarm line violations can serve as a quick check of test quality before concluding a vibration test. This metric is calculated by summing all control frequency lines outside of the abort/alarm limits, and normalizing by the total number of lines. Table 3 summarizes the abort/alarm line performance of our MIMO tests.

Table 3 is shaded in a similar fashion to Table 2, where green cells represent better performance, and red cells represent poorer performance. The stiffened MIMO test again performed the worst by a large margin. The remaining tests, however, do not show a large difference in control performance. This metric was more rigorous for the stiffened/truncated MIMO test because the limited frequency range reduces the number of spectral lines for normalization. Therefore, it takes fewer violations to get the same % error as the other tests with full ranges. Despite this, the differences in abort violations between the undamped, damped, and stiffened/truncated MIMO tests were less than 1%. Comparing the alarm violations for these tests, the error was larger, but the maximum difference between configurations was still only around 1%. The threshold for

Table 2 The gRMS % Error scores for the four MIMO test at each control DOF

		gRMS		
Configuration	**Control DOF**	**Control**	**Test Specification**	**% Error**
Undamped	23	0.597	0.571	4.6
	26	0.586	0.571	2.6
Damped	23	0.559	0.571	2.1
	26	0.560	0.571	1.9
Stiffened	23	0.651	0.571	14.0
	26	0.662	0.571	15.9
Stiffened/Truncated	23	0.466	0.473	1.5
	26	0.457	0.473	3.4

Table 3 The % abort/alarm line violation scores for the four MIMO test at each control DOF

		% Violation	
Configuration	**Control DOF**	**Alarm**	**Abort**
Undamped	23	0.63	0.20
	26	0.47	0.12
Damped	23	0.71	0.12
	26	0.39	0.00
Stiffened	23	7.57	2.88
	26	10.37	3.75
Stiffened/Truncated	23	1.72	0.00
	26	0.60	0.00

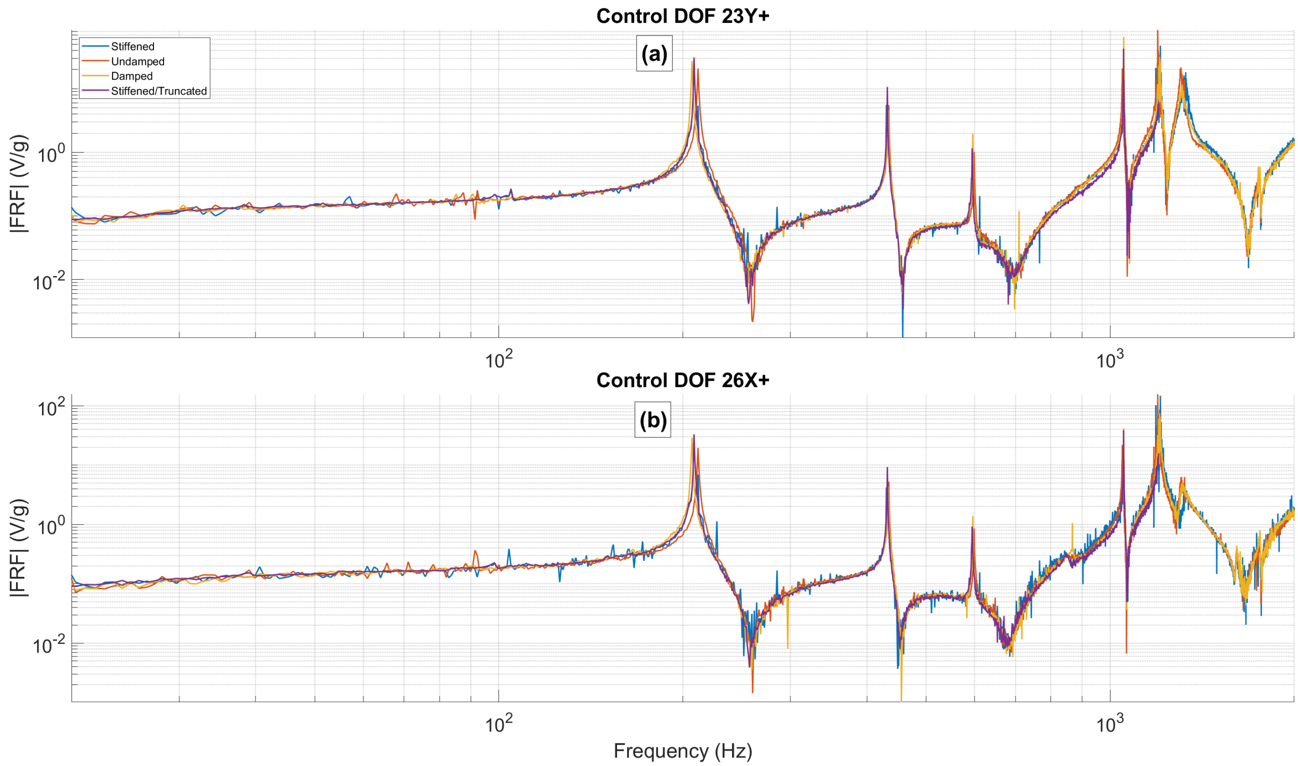

Fig. 8 The inverse FRFs reported by Testlab 2021.2.1 for the four MIMO tests: (a) inverse FRFs for control DOF 23Y+, (b) inverse FRFs for control DOF 26X+

alarm/abort line violations is 5% and 2% respectively. The undamped, damped, and stiffened/truncated MIMO tests were again well below these thresholds. The results from this metric agree with our findings from the previous metric, suggesting little impact from the test stand on the MIMO tests.

Inverse FRF Comparison

Our previous results showed that the dynamics of the test stand in the range of identified modes (20-300 Hz) did not appear to influence the control performance of the MIMO tests. However, the question remained whether the controller overcame the test stand dynamics, or was not affected by them at all. To understand the impact the test stand dynamics on the controller, we analyzed the inverse FRFs between the control DOFs and input voltage from our MIMO tests. These FRFs inform the controller's decisions concerning how much voltage to apply to get a desired acceleration response. Resonances from the test stand would appear in the inverse FRFs as peaks and valleys if the controller were making an effort to overcome them. Figure 8 plots the inverse FRFs reported by the Testlab 2021.2.1 MIMO random module for each of the MIMO test cases.

The inverse FRFs from Figure 8 were relatively flat in the range of 20-200 Hz, where many of our identified test stand modes lie (16-25 modes depending on the test stand configuration). Since there were no peaks or valleys, one can conclude that the test stand resonances had no noticeable impact on the controller in this range. It is observed that there was a resonance and anti-resonance in the inverse FRF between 200-300Hz, and the test stand had resonances in this range. However, if this behavior were caused by variations in the test stand, it would be expected that the inverse FRF would vary between configurations. Instead, the system dynamics had almost *no* change from test to test. The inverse system FRFs were nearly identical regardless of test stand configuration. This implies that the behavior of the test article, as a result of the shaker input, was independent of the test stand dynamics.

The inverse FRFs, see Figure 8b, were observed to have more distortion than the curves in Figure 8a. The audible rattling describe in earlier sections emanated from the shaker located at DOF 26X+. This rattling increased the level of noise in the measured data, and was likely the cause of the added distortion. Because the distortion appears in all of the curves, the rattling may have been a issue in all of the MIMO tests, progressively getting worse until the controller could no longer handle it in the stiffened MIMO test. Limiting the frequency range of the stiffened/truncated MIMO test cut off the rattle frequency, and allowed the controller to replicate the specification with greater accuracy.

Discussion and Conclusion

Performing a modal test on a test stand can be a useful tool for understanding at what frequencies test stand resonances occur. Identifying these resonances can give the test engineer confidence in determining whether undesirable control performance was caused by the test article or the test stand. From the high modal density in the low frequency range to the high compliance from the transmissibility plots, our test stand exhibited many undesirable behaviors. Based on these observations, we expected that the resonances of the test stand would negatively impact our MIMO control. However, this expectation was not substantiated by the experimental evidence. Instead, our analyses indicated that the dynamics of the test stand had little discernible impact on our MIMO tests in this case. Furthermore, the lightly damped resonances of the test article were the single biggest contributor to poor MIMO control.

This study analyzed a modular test stand for random MAVT. Three test configurations were analyzed, with each intended to be an improvement on the last. We began by performing impact hammer tests on each configuration and extracting the mode shapes. From comparison of the mode shapes via the MAC, we concluded that five of the modes from the undamped configuration were split in the damped configuration. The TR was approximated for each test configuration to capture the rigidity of the configurations. The TR plots indicated that adding stiffening improved the rigidity of the test stand, but did not eliminate compliance. The test article used in MIMO testing was also impact tested and its mode shapes extracted. The test article had eight lightly damped modes in our frequency range of interest, i.e. the frequencies 20-2000 Hz.

We then compared the MIMO test performance of the various test configurations. The stiffened MIMO test performed poorly, likely due to unwanted rattling and displacement of the test article. The other three MIMO tests satisfied our success criteria. The inverse FRFs from our MIMO tests indicated that there was little dynamic change to the shaker-test article dynamics between the test stand configurations. We therefore concluded that the dynamics of our test stand had little to no effect on the control effort in the MIMO tests. Additionally, the dynamics of the test article were the greatest contributing factor in test specification adherence.

We do not claim that these findings will be the case for all test stands used in random MAVT. Other important considerations include the weight of the test article, the size of the shakers, characteristics of the test specification, and the geometry of the test stand. Future work is needed to understand how these factors may impact MIMO test performance and shaker-stand coupling.

Acknowledgments This research was supported by the Delivery Environments program under the Office of Engineering and Technology Maturation at Los Alamos National Laboratory (LA-UR-24-30436).

References

1. Rohe, D.P., Nelson, G.D., and Schultz, R.A. "Strategies for shaker placement for impedance-matched multi-axis testing". In *Sensors and Instrumentation, Aircraft/Aerospace, Energy Harvesting & Dynamic Environments Testing, Volume 7: Proceedings of the 37th IMAC, A Conference and Exposition on Structural Dynamics 2019*, pages 195–212. Springer (2020)
2. Mayes, R., Ankers, L., Daborn, P., Moulder, T., and Ind, P. "Optimization of shaker locations for multiple shaker environmental testing". *Experimental Techniques*, 44:283–297 (2020)
3. Daborn, P.M., Roberts, C., Ewins, D., and Ind, P. "Next-generation random vibration tests". In *Topics in Modal Analysis II, Volume 8: Proceedings of the 32nd IMAC, A Conference and Exposition on Structural Dynamics, 2014*, pages 397–410. Springer (2014)
4. Avitabile, P. "Why you can't ignore those vibration fixture resonances". *Sound and Vibration*, 33:20–27 (1999)
5. Trubert, M. "Structural and electromechanical interaction in the multiple-exciter technique for random vibration testing". *The Journal of the Acoustical Society of America*, 41(5):1185–1192 (1967)
6. Peres, M., Bono, R., and Avitabile, P. "Effects of shaker, stinger and transducer mounting on measured frequency response functions". *The 25th Intenational Conferenece on Noise and Vibration Engineering ISMA-USD*, pages 1475–1490 (2012)
7. Varoto, P.S. and de Oliveira, L.P. "Interaction between a vibration exciter and the structure under test". *Sound and vibration*, 36(10):20–26 (2002)
8. Siswanto, W.A., Ibrahim, M.N., Madlan, M.A., and Mohamad, S.M. "Shaker table design for electronic device vibration test system". *International Journal of Engineering and Technology*, 3(6):663 (2011)
9. Peres, M.A., Bono, R.W., and Brown, D.L. "Practical aspects of shaker measurements for modal testing". In *Proceedings of the ISMA*, volume 1105, pages 2539–2550 (2010)
10. Pastor, M., Binda, M., and Harčarik, T. "Modal assurance criterion". *Procedia Engineering*, 48:543–548 (2012) Modelling of Mechanical and Mechatronics Systems.
11. U.S. Dept. of Defence, Washington, DC, USA. *MIL-STD-810H* (2019)

Appendix

Table 4 The modal frequencies for the three test stand configurations and test article

	Frequency (Hz)			
Mode Number	**Undamped**	**Damped**	**Stiffened**	**AL Angle**
1	29.4	28.7	38.8	323.8
2	32.1	30.8	39.2	501.7
3	39.2	36.0	51.4	679.1
4	68.8	37.4	75.5	1100.4
5	70.9	66.4	79.5	1643.9
6	88.5	67.0	99.4	1694.6
7	93.0	68.2	104.8	1772.0
8	101.9	68.9	105.1	1909.4
9	111.2	86.2	114.7	-
10	126.9	91.5	115.2	-
11	137.8	96.1	144.4	-
12	151.4	97.0	151.6	-
13	154.6	104.4	165.0	-
14	157.9	105.0	171.6	-
15	168.9	110.8	180.8	-
16	175.1	123.0	187.5	-
17	185.3	140.5	201.6	-
18	209.5	146.6	205.9	-
19	255.3	148.9	225.2	-
20	-	161.3	237.9	-
21	-	162.7	264.6	-
22	-	164.2	271.3	-
23	-	168.9	276.1	-
24	-	171.2	279.5	-
25	-	194.7	-	-
26	-	222.2	-	-
27	-	232.3	-	-
28	-	245.3	-	-